Kimiabeigi M, Widmer JD, Long R, Gao Y, Goss J, Martin R, Lisle T, Vizan JMS, Michaelides A, Mecrow BC.

On Selection of Rotor Support Material for a Ferrite Magnet Spoke-Type Traction Motor.

***IEEE Transactions on Industry Applications* 2016, 52(3), 2224-2233.**

DOI link to article:

http://dx.doi.org/10.1109/TIA.2016.2530722

Date deposited:

14/07/2016

On Selection of Rotor Support Material for a Ferrite Magnet Spoke Type Traction Motor

M. Kimiabeigi, J. D. Widmer, R. Long, Y. Gao, J. Goss, R. Martin, T. Lisle, A. Michaelides, B. Mecrow

***Abstract*—Interior permanent magnet motors with ferrite magnets and distributed windings can be a cost effective alternative to rare-earth magnet based motors for demanding applications such as automotive traction. Among different rotor topologies, the spoke type may be preferred, due to its advantages for high flux concentration and resistance to demagnetization, when carefully designed. When high speed operation is required, to increase the power density of the motor, the spoke type rotor must comprise of two sections: a) the ferromagnetic rotor pole to provide the path for the magnetic flux, and b) the non-magnetic rotor support to provide the structural integrity. In this paper, the multiphysics and cost implications of the rotor support material, as part of a high performance ferrite magnet traction motor, are analyzed, and an optimal selection with respect to those criteria is proposed. The performance of the design based on the proposed rotor support material is validated by electromagnetic and structural testing of three sets of customized prototypes. Based on the analysis, the proposed rotor support material may, significantly, boost the cost competitiveness of a low cost ferrite motor for high volume production.**

***Index Terms*-- Austenitic Steel, Electric Vehicle (EV), Ferrite Magnet, High Speed, Rotor Support, Spoke.**

I. Introduction

PERMANENT magnet (PM) motors using rare earth magnets, such as Neodymium Iron Boron (NdFeB), may provide a high torque density and high efficiency solution for demanding applications such as automotive. However, due to the high and unstable cost of the rare-earth material, the research toward using alternative and cheaper grade of magnets, such as those with lower levels of Dysprosium or ferrite magnets, has, recently, become popular, [1], [2], [3]. To meet the design challenges when using poor ferrite magnets (with low levels of remanent flux density, B_r, and intrinsic coercivity, H_{cj}) a combination of multi-physics based techniques must be applied, which, ultimately, may limit the feasible design variations to few topologies, including Flux Switching PM (FSPM) machines, [4], Permanent Magnet Assisted Synchronous Reluctance type (PMASynR) with U shape or V shape topology magnet and flux barrier layers, [5]-[10], and spoke type rotors, [11-17].

To compensate for the low B_r levels, the ferrite magnets are usually arranged in oriented planes to achieve flux concentration effects, [12], [13], while, additionally, due to the salient structure of the PMASynR or spoke type rotor, significant contribution of the reluctance torque may be achievable, [7], [8]. To deal with the high demagnetization risk of the ferrite magnets due to the relatively low levels of H_{cj}, the rotor flux barriers are usually tapered toward the airgap, [7], or in case of spoke type rotors, non-magnetic regions on top and bottom of the magnets can be provided, [17]. Furthermore, in [14] it is shown that extruding the magnets beyond the stator stack may assist demagnetization, while in [10] an analytical tool to derive the safe operating current (i.e. the current under which the magnets are safe from demagnetization) is presented.

When choosing a rotor with spoke topology, the rotor structure may be composed of a single piece lamination stack [16]. In this configuration, the appropriate flux barriers must be designed to avoid an excessive permanent magnet flux leakage through the rotor yoke, as well as providing a sufficient structural integrity for operation at high speeds. Another viable spoke type configuration includes a rotor comprised of two sections, [15], [17]: a) the rotor poles made of ferromagnetic laminations which provide the magnetic flux path, and b) the rotor support made of a non-magnetic and sufficiently strong material which holds the rotor poles and provide the rotor integrity via a so-called fir-tree feature, [18]. Although, the single piece rotor topology may be advantageous over the fir-tree based type, due to its simplicity and having fewer components, the latter may be preferred due to its superior performance both magnetically (due to less magnet leakage through the rotor yoke) and structurally, which facilitates the operation at higher speed and achieving higher power densities.

Despite the high performance of the state of the art example in [15], the rotor support of this design is made of copper beryllium. Beryllium is an element with high strength and low weight and results in excellent structural and formability of the associated alloys including copper beryllium, [19]-[22]. However, this element is, relatively, scarce in the earth crust, with the US accounting for about 65% of the resources and 90% of the global production in 2014, [20]. Furthermore, the mining and production of Beryllium alloys might be associated with some health and environmental hazards, [21], [22]. As a result, in this paper, a high performance ferrite spoke design, disclosed in [17], is, majorly, analyzed with regards to an optimal choice of the rotor support material. The analysis includes a comparison of the motor multi-physical performance based on a few viable rotor support materials, in particular

The project is funded by Innovate UK under Grant 110130.

M. Kimiabeigi, J. D. Widmer, R. Martin, T. Lisle, and B. Mecrow are with Newcastle University, NE17RU, UK (mohammad.kimiabeigi@ncl.ac.uk); R. Long and Y. Gao are with Tata Steel, UK; James Goss is with Motor Design Ltd, UK; A. Michaelides is with Jaguar Land Rover, Gaydon, UK.

different grades of austenitic steels. The aim of the studies is to propose and assess the implications of using austenitic steel (as a cheaper and more widely available alternative to copper beryllium) suited to low cost high performance ferrite motors, in particular for high volume productions.

II. Ferrite Based Spoke Type Motor with Distributed Winding

As part of an Electric Vehicle (EV) project, with the major requirements presented in Table I, and following a multi-objective multi-physical optimization procedure, a spoke type motor with ferrite magnets and distributed windings has been designed and reported in [17]. The major dimensions as well as the two dimensional (2D) topology are shown in Table II and Fig. 1, respectively. To cope with the structural requirements at high speed, the rotor is composed of two parts which are joined via a fir tree root, Fig. 1. The performance in terms of the peak transient torque at base and top speed, as well as the effects from the rotor skew, are shown in Fig. 2, where the base value of 1 per unit corresponds to 270 Nm.

TABLE I
DESIGN REQUIREMENTS FOR THE FERRITE BASED TRACTION MOTOR.

Available volume (cylinder)	< 14 liter
Peak power density	>6 kW/liter
Continuous power density	>4 kW/liter
Base to top speed ratio	3000 rpm : 15000 rpm
Maximum winding temperature	180 ˚C
Available water cooling options	Only via outer stator frame
Demagnetization withstand capability	Against 3-phase short circuit
Maximum achievable inverter current, I_{pk}	420 Arms
Minimum available DC link voltage	400 V
FB9B Ferrite, B_r at 20˚C/ H_{cj} at 20˚C	0.44 T/ 370 kA/m

TABLE II
Major dimensions of the spoke type design.

Stator outer diameter (mm)	205
Rotor outer diameter (mm)	140
Stack length (mm)	195
Airgap (mm)	0.5

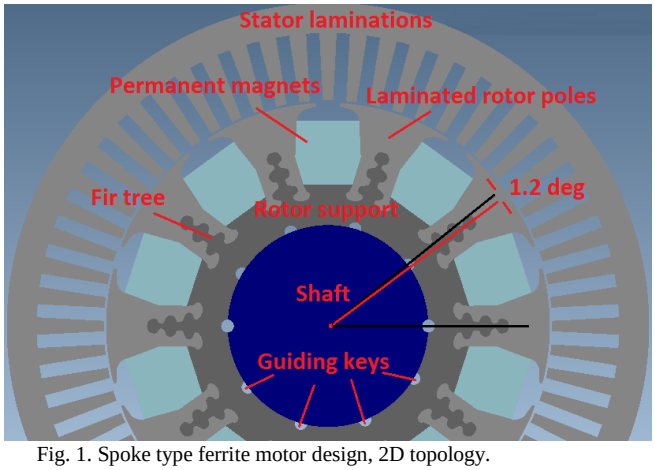

Fig. 1. Spoke type ferrite motor design, 2D topology.

Despite an independent development of the rotor design in [17], some geometrical similarities with that in [15] have occurred, which is, mainly, due to some similar project constraints and targets, such as similar base and top speed, and the target of achieving maximum power density and efficiency in both designs. As a result of the multi-physical optimization, [17], it has been concluded that a spoke type design at the specified high speed levels need to be composed of a fir-tree and rotor support structure, to cope with the high structural stress as well as fulfilling the maximum achievable power density (the fir tree design has superior magnetic performance compared to the single piece alternative, due to the less magnet leakage through the rotor yoke). With regards to the fir tree topology, based on the structural optimization, it was realized that the higher number of fir tree teeth, i.e. 6 vs. 3 teeth, [17], results in slightly better structural performance, however the fewer number was, ultimately, selected due to its simplicity for the high volume manufacturing. It should be mentioned that due to the minor differences between the aforementioned numbers of the fir tree teeth in terms of the structural performance, more variations have not been investigated.

The disclosed rotor in [17] is composed of five axial sections which are skewed in four steps, and according to an innovative pattern of ten guiding keys, Fig. 1, half of which are distant by an angle equal to $360/P + \alpha/(m-1)$, (P is the pole number, α is the total angle of skew and m is the number of rotor axial sections, i.e. 5), while forming a diametrical symmetry with the remaining five keys (each of the five rotor sections is fitted to the shaft via a diametrical pair of the keys during the assembly, resulting in a complete four step skewed rotor). The aforementioned arrangement prevents the multiplication of the rotor segment parts (all rotor segments have the identical topology shown in Fig. 1) and, thereby, does not increase the manufacturing and assembly costs for a high volume production. Some other distinctive features of the rotor design in [17] include the parallel sided magnets on top, which may allow for better magnet tolerances and, thereby, lower magnet costs. Finally, through an innovative approach (beyond the scope of this paper) the clearance between the rotor poles and rotor supports has been minimized, in such a way that the rotor components fit more closely and robustly together, improving the rotor integrity during the high speed operation.

With regards to the stator, the windings are made of aluminum to save weight and cost, while the wires sizes and geometry are, optimally, chosen to maximize the slot fill factor, and minimize the AC losses during high speed operation. A detailed investigation of the windings and comparison of the aluminum and copper in terms of the magnetic and thermal performance will be presented in a separate paper.

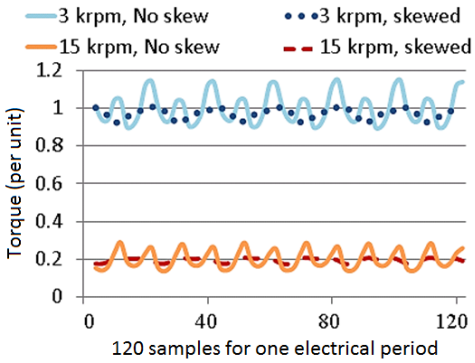

Fig. 2. Optimal spoke type design, torque and ripple waveform with and without skew.

In the following sections, and as the main objective of this paper, the influence of the rotor support material on the

multi-physical performance and cost of the ferrite motor design in [17] is studied in details.

III. Rotor Support Multi-physical Requirements and Viable Material Options

A. Structural Considerations

1) Mechanical and fatigue properties

To achieve the optimal fir-tree design in Fig. 1, a series of structural-magnetic optimizations have been made, using 2D FE tools; the objective was to control the peak stress below the tensile and fatigue limits of the rotor pole and rotor support materials. A schematic illustration of a tensile stress-strain curve and the associated physical parameters is shown in Fig. 3.

Some of the early generations of fir tree design are shown in Fig. 4, where some optimization outcomes such as increasing the bubble cut-out radius, or adjustment of the circumferential teeth height are illustrated. In the design corresponding to Fig. 4(b), the two top circular cavities, see Fig. 4(a), have been removed to increase the quadrature-axis inductance and the reluctance torque. The design in Fig. 4(b) is further modified and re-optimized by reducing the number of fir tree teeth from 6 to 3, Fig. 5, to facilitate the tolerance and manufacturability aspects, while as a result of the process a 3% loss of the peak torque was realized.

The stress distributions in the rotor pole and the rotor support of the latest fir tree generation are shown in Fig. 5 (half a pole is shown due to symmetry), where 316L austenitic steel with 3% work hardening, and M270-35A non-grain oriented electrical steel are, respectively, used for the rotor support and the rotor pole. From Fig. 5, the maximum stress values in the poles and the rotor support are within the acceptable fatigue limits of their respective materials (i.e. to ensure a life time longer than the vehicle).

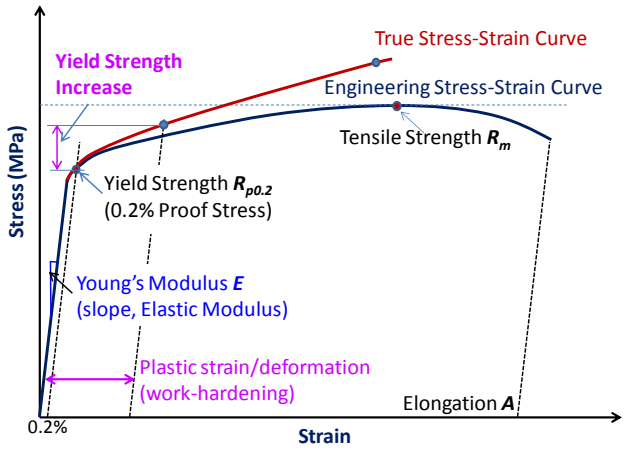

Fig. 3. Illustration of tensile stress-strain curve.

2) Work hardening and Young's modulus

A metal's effective yield strength often increases after it has been subjected to a certain level of plastic deformation, e.g. 2–5% plastic strain. This is known as work hardening or strain hardening. The mechanism of the work-hardening-induced increase in effective yield strength is illustrated in Fig. 3. From a structural point of view, work-hardening often brings about the same benefit as selecting a higher-strength material.

Another important mechanical property is Young's Modulus, or Elastic Modulus (E), see Fig. 3. There is little difference among steels of various kinds, having a Young's modulus value range of 185 – 210 GPa at room temperature. On the other hand, aluminum alloys have a much lower Young's modulus of ≈70 GPa; finally the copper beryllium can be ranked between the steels and aluminum, having a Young's modulus of ≈128 GPa.

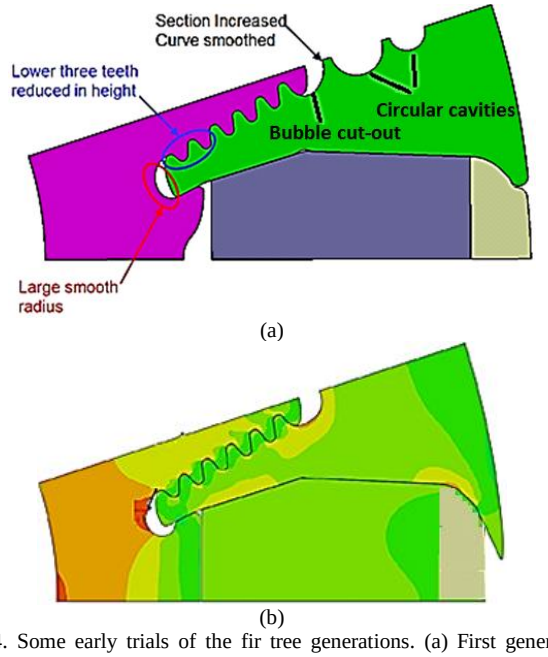

Fig. 4. Some early trials of the fir tree generations. (a) First generation design with circular cavities, and some optimization hints. (b) Second generation design.

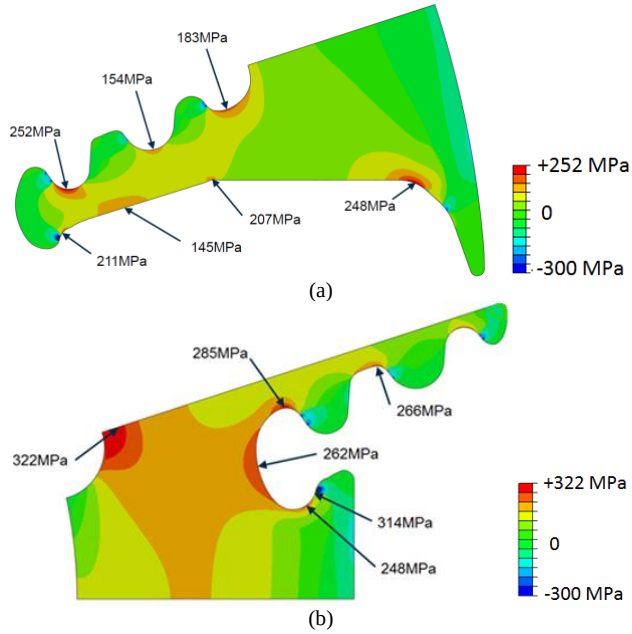

Fig. 5. Stress distributions at 15 krpm, non-work hardened austenitic steel 316L. (a) Rotor pole. (b) Rotor support.

Fig. 6 shows the effects of Young's modulus and yield strength of various rotor support materials on another important rotor structural parameter, namely the radial expansion. High-speed rotor radial expansion will have a direct impact on a motor's operating rotor-stator air-gap. In the current study, radial expansion levels of a number of different rotor support materials, including austenitic 316L (non-work hardened and 3% work hardened) and a higher-strength Nitronic 50 stainless steel, a strong aluminum alloy 2024-T3, and finally copper beryllium were evaluated by

finite element (FE) analyses. The speeds between 15 krpm to 18 krpm account for the 20% over speed requirement.

As can be seen in Fig. 6, due to their lower Young's modulus, both aluminum (to higher degree) and copper beryllium (to lower degree) rotor supports would produce higher radial expansion levels than those of stainless-steel supports. Among stainless-steel rotor supports, radial expansions are similar until the rotor speed reaches about 16.5krpm, when non-work-hardened 316 stainless steel starts to yield and cause the rotor radial expansion to increase sharply. Between the higher-strength Nitronic 50 and the work-hardened stainless steel 316L (with 3% plastic strain), there is very little difference in terms of rotor radial expansions. In fact, a more detailed examination indicates that the 3% work-hardened 316L produces a slightly lower rotor radial expansion than that of a Nitronic 50 rotor.

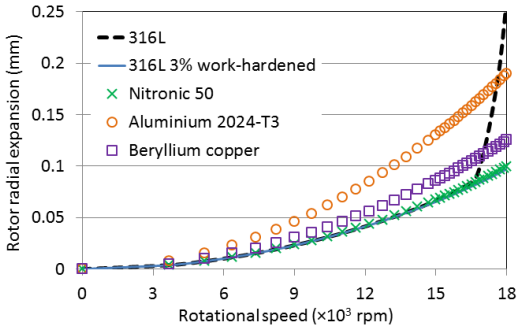

Fig. 6. Comparison of rotor radial expansions for various rotor support materials.

3) Potential issues with work hardened stainless steels

The strength increase due to work hardening is not always stable, especially if the material is to be exposed to elevated temperatures. In addition, work-hardening may lead to changes in other aspects of the material, such as in microstructure and in other physical and magnetic properties. One potential issue with work-hardening of austenitic steels is the risk of regaining some magnetism. This is due to partial transformation of austenitic phase into martensite as a result of plastic deformation, [23]. The level of regained magnetism depends on the steel grade, plastic strain levels and, ultimately, on the chemical composition and homogeneity of the material, [24].

For the current rotor design and based on the plastic deformation and fatigue endurance requirements, a rotor support material with minimum yield strength and fatigue limit (fully-reversed cyclic loading) of, respectively, 290 MPA and 270 MPa is needed. The yield strength limit is based on the strain calculations in the materials and the requirement to avoid permanent deformation under zero to 18 krpm over-speed requirement; Fig. 6 illustrates an example of an excessive plastic deformation in the non-work hardened 316L steel rotor support due to its insufficient yield strength. Furthermore, the indicated fatigue limit is based on the cyclic stress variation in the rotor support under normal operational range of speed, i.e. zero to 15 krpm, and according to the number of cycles to failure data of the material, [25], it ensures a rotor life time longer than the expected life time of the vehicle.

These requirements are slightly above the capability of non-work hardened 316L steel. The UTS and yield strength of some grades of austenitic steels, with and without work-hardening, are summarized in Table III, [26]. Furthermore, in Fig. 7 the magnetic permeability of these grades for different levels of work hardening is shown, [27], where a homogenous material composition has been assumed. From Table III and Fig. 7, it can be realized that: a) In the case of 302 and 304 austenitic steels by small to medium levels of work-hardening (up to 40%), the mechanical property of the steel can, significantly, be improved, while no regain of magnetism is expected; b) In the case of 316L grade, while the mechanical property can, significantly, be improved by work-hardening, the martensitic phase conversion is quite negligible, even for very high levels of work-hardening.

B. Magnetic Analysis

To assess the effect of rotor support magnetic property on the motor performance, the maximum torque at base and top speed was simulated using 2D FE, and shown in Fig. 8. As illustrated in Fig. 8, it can be realized that even for a small increase in magnetic permeability of the rotor support, the maximum torque capability of the motor might be significantly reduced, due to the excessive flux leakage through the rotor support. However, as explained in Section A, due to the very low level of work-hardening required to achieve the requirements of the rotor design in Fig. 5, most grades of austenitic steel (316L in particular) are expected to fully retain their non-magnetic property, resulting in no degradation of the electromagnetic performance.

TABLE III
CHANGE OF UTS AND YIELD STRENGTH VS. WORK HARDENING, [26].

	Percentage of work hardening					
	0	10%	20%	30%	40%	50%
302 SS						
Tensile	642	745	842	952	1049	1159
Yield	255	628	738	828	925	1014
304 SS						
Tensile	593	676	780	897	1007	1090
Yield	235	476	738	828	932	1001
316L SS						
Tensile	587	656	759	897	980	1035
Yield	262	483	676	814	883	945

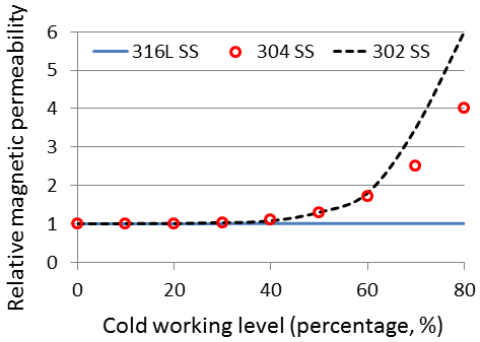

Fig. 7. Change of magnetic permeability vs. work hardening, [27].

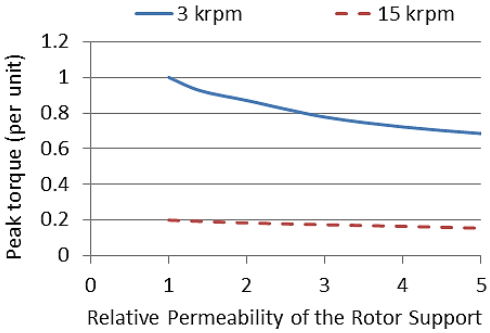

Fig. 8. Peak torque capability at base and top speed vs. rotor support permeability.

C. Thermal Performance

1) Electromagnetic losses

The electromagnetic losses in the rotor of a PM machine are due to the magnetic field harmonics that rotate asynchronously to the rotor. As reported in [28], the designs with fractional slot windings are known to experience higher rotor losses compared to those with distributed windings, due to the rich Magneto Motive Force (MMF) harmonic and sub-harmonic contents inherent in this type of windings.

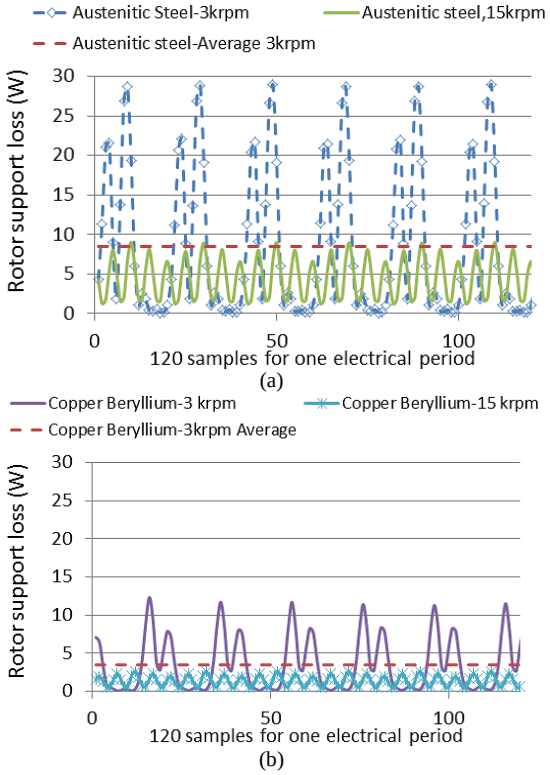

Fig. 9. Rotor support losses for the peak power operating points at 3 krpm and 15 krpm rotor speeds. (a) Austenitic steel rotor support. (b) Copper beryllium rotor support.

The rotor support losses for both copper beryllium (conductivity of $1.16 * 10^7\ S/m$), and austenitic steel (conductivity of $1.4 * 10^6\ S/m$) have been calculated using FE 2D. In these calculations, the rotor support is assumed as a solid conductor piece, and only the z-axis component of the eddy currents is taken into account. Based on the results in Fig. 9, despite the higher conductivity of the copper beryllium, the average rotor support losses are about half the losses with austenitic steel, which is due to the stronger skin/ shielding effect of the copper. However, for both materials the rotor support loss is quite negligible, i.e. less than 0.1% of the winding loss at the same operating point; as a result, regardless of the materials the rotor support losses has a negligible impact on the efficiency of the motor. An illustration of the loss in the austenitic steel rotor support (at a rotor position corresponding to the maximum loss) is given in Fig. 10, from which it can be realized that the losses are largest in the regions beneath the magnets where the maximum variation of the flux occurs.

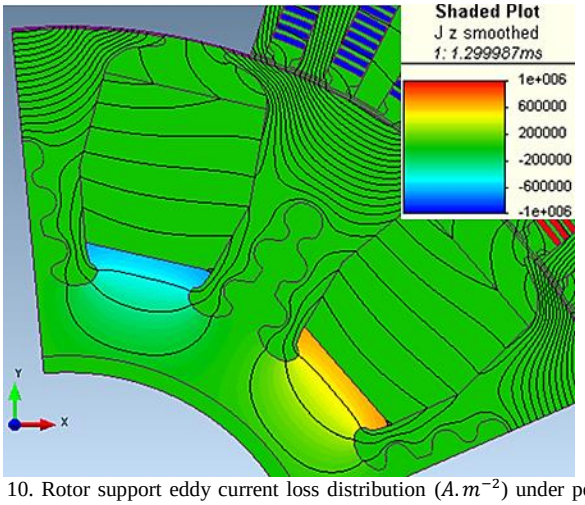

Fig. 10. Rotor support eddy current loss distribution ($A.m^{-2}$) under peak load- 3000 rpm operation, austenitic steel.

2) Cooling

Due to the higher thermal conductivity of the copper beryllium compared to the Austenitic steel (200 W/m.K vs. 15 W/m.K), the former might be a preferable option in designs where liquid cooling via the shaft, such as in [29], is intended. However, in designs with other methods of cooling, such as the one in [17], where the source of heat exchange is located on the outer stator frame, the thermal characteristics of the rotor support would have minimal influences on the general thermal performance. To demonstrate this, the stator winding and the magnet temperature are simulated at two representative operating conditions, Fig. 11: a) a continuous operation at 60 kW and 10 krpm (i.e. a relatively, high power and high speed) to represent a severe thermal loading, and b) a continuous operation at 10 kW and 6 krpm (a key operating point according to the vehicle drive cycle) to represent a thermal loading that determines the motor efficiency. As seen in Fig. 11, the thermal behavior is, almost, identical for the two rotor support materials. It should be noted that in [15], even though no direct shaft cooling is applied, the rotor support material is kept the same as in [29], i.e. copper beryllium; this choice would impose an unnecessary high cost penalty that will be discussed in Section D.

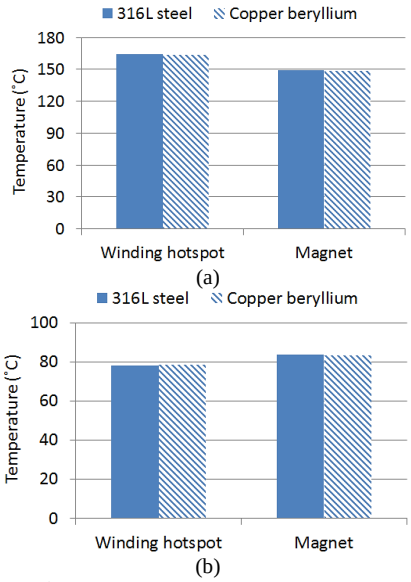

Fig. 11. Effect of rotor support material on the winding and magnet temperature. (a) Continuous operation at 60 kW, 10 krpm. (b) Continuous operation at 10 kW, 6 krpm.

D. Cost

A major motivation for ferrite based designs is to reduce the overall cost of the motor. Thereby, careful material selection must ensure that such designs do not lose their competitiveness against rare-earth magnet alternatives. The costs of the rotor support for different grades of steel and copper beryllium have been quoted and estimated based on several sources including [20], [30], [31], [32], assuming a volume production of 100,000 motors per year, and are normalized based on the cost of the ferrite magnets used per motor volume; the results are shown in Fig. 12. With regards to copper beryllium, the price is based on ~2% contained beryllium, while the final product price (in contrast to the raw material price indicated in [20]) has been considered. Furthermore, based on quotes from different sources a rather large variation of price can be obtained, as indicated in Fig. 12.

Based on Fig. 12, it is clear that, a) the cheapest option that fulfills the structural requirements in Section A, is the 3% work hardened 316L austenitic steel, the cost of which is 120% of the cost of the ferrite magnets, b) work hardened steel is significantly cheaper than using a stronger grade of steel, such as Nitronic 50, and c) the copper beryllium can be 3~6 times more expensive than the proposed austenitic steel option (depending on the steel grade and subject to variation of quotes), and, can constitute a cost up to 600% of the total magnet costs, which might compromise the performance per cost competitiveness of the ferrite based designs.

Finally, it should be mentioned that along with the selection of the rotor support raw material, care must be taken to avoid costly manufacturing techniques. Due to the excellent forming quality of the copper beryllium, it can be extruded to the required shape. In case of steel, due to limitations of extrusion and high costs of machining, alternative methods should be sought which is currently under investigation.

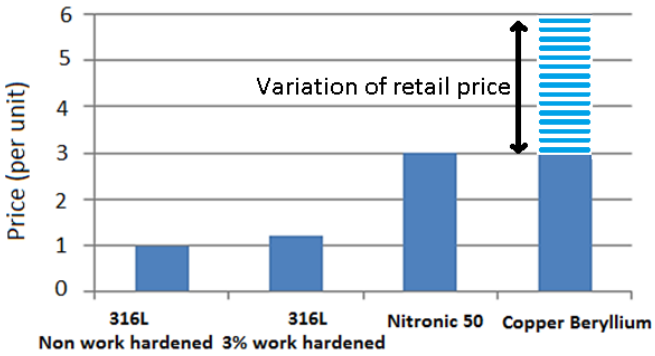

Fig. 12. Price comparisons for the different rotor support materials.

IV. Prototype Test

Due to difficulties in procuring low volumes of work hardened stainless steel, the more readily available Nitronic 50 (with similar magnetic and structural properties as 3% work hardened steel) was used for the prototype testing. A component view of the rotor and stator can be found in [17], while the full size prototype set is shown and compared against the Nissan Leaf motor in Fig. 13. As discussed in [17], the prototype ferrite motor has a very similar envelope as the rare earth magnet design in Leaf, which allows for a better evaluation of the ferrite based design.

The Back-EMF (BEMF) of the prototype motor is measured at the 20 ˚C room temperature and a fixed rotor speed, corresponding to 33 Hz electrical frequency, and shown in Fig. 14(a). Furthermore, the fundamental component is linearly scaled against the rotor speed and compared against the FE 3D simulations, in Fig. 14(b). From Fig. 14(a) and (b), it can be realized that the BEMF is close to sinusoidal, due to the rotor skew, while there is a 7% difference between the measurement and the FE predictions, which can be majorly attributed to the manufacturing tolerances such as the small gaps between the magnets and the rotor pole, which were neglected in the FE modelling.

The static torque of the prototype motor has been measured using a test set up shown in Fig. 15 and shown against the stator current in Fig. 16. It should be noted that a water cooling system was applied to maintain a constant rotor temperature of ~ 70 ˚C throughout the test. Based on Fig. 16, the torque follows a quasi-square function at lower current levels (due to the high reluctance torque contribution) while at larger currents the rate of increase is diminished due to the magnetic saturation. Furthermore, there is an 8% difference between the measurement and the FE 3D results, which is similar to the BEMF findings.

Based on the results obtained from the BEMF and static torque testing, and considering a 14 liter gross volume for both ferrite and Leaf design (including the cooling housing and end windings), the prototype in Fig. 13 may deliver a peak torque and power density of up to 18 Nm/ liter (about 90% of the Leaf motor rating) and 5.6 kW/ liter at 3000 rpm base speed (about 98% of the Leaf motor rating). To assess these values under running conditions, a more comprehensive testing of the prototype motor using the full size inverter and under different rotor speeds is, currently, under investigation.

Finally, it should be noted that to demonstrate the non-magnetic properties of the austenitic steel applied in the prototype motor, the scaled prototype version in [17], has been fitted with aluminum rotor support, for which the BEMF and torque measurements were found to be identical to the ones fitted with austenitic steel rotor supports.

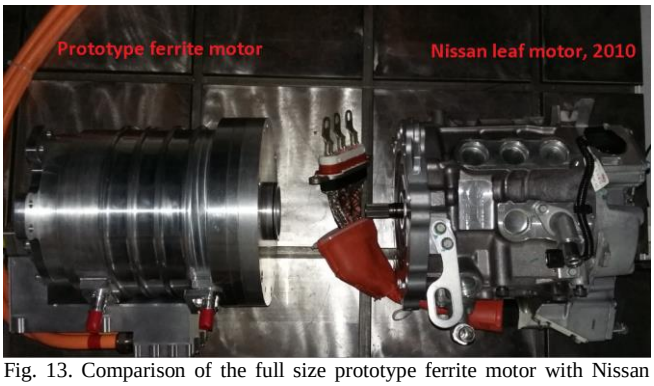

Fig. 13. Comparison of the full size prototype ferrite motor with Nissan leaf motor.

To validate the structural integrity of the rotor and safety of the operation at high speeds, another customized prototype has been built, Fig. 17(a). As shown in Fig. 17(a), this prototype comprises of two out of the five rotor axial segments (each of which has one fifth of the reference design stack length), which are skewed according to $\alpha/(m-1)$, α being the total angle of skew equal to 4.8 degree, and m equal to total number of rotor axial segments,

i.e. 5. The rotor is further completed with the high speed bearing, and embedded within two sets of protective housing which were securely bolted to the test bed plate and into the concrete ground, Fig. 17(b). Based on the results from the high speed testing, the prototype rotor proved to be capable of safely operating at 120% of the top speed, with no sign of plastic deformation (based on an accurate measurement and comparison of the rotor diameter before and after the test) or loosening of the fasteners being recorded.

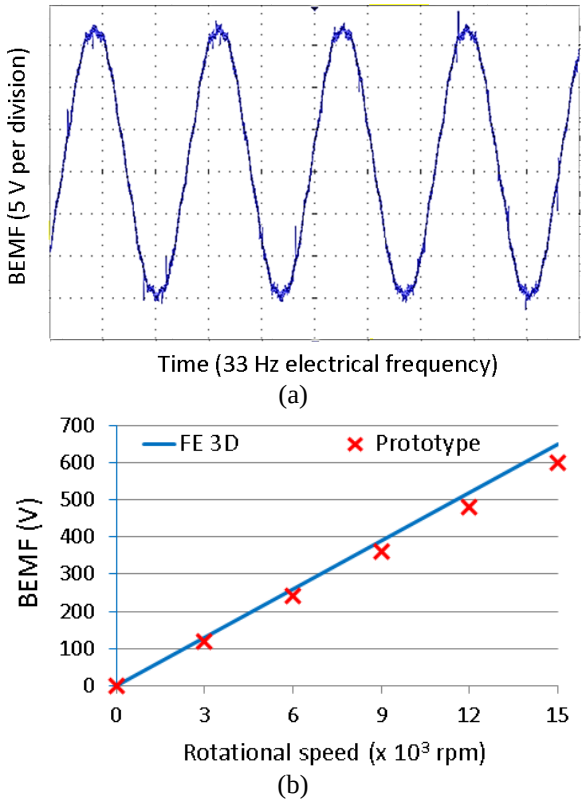

Fig. 14. BEMF testing. (a) Prototype BEMF measurement at 33 Hz electrical frequency. (b) BEMF vs. rotor speed.

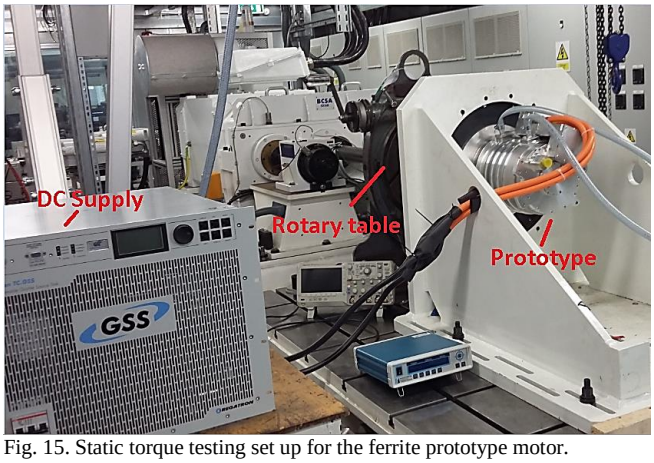

Fig. 15. Static torque testing set up for the ferrite prototype motor.

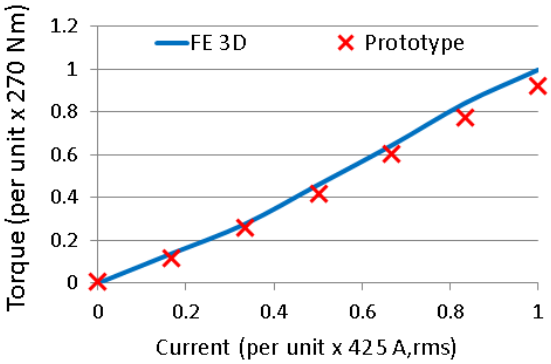

Fig. 16. Static torque against current; prototype testing vs. 3D FE simulation.

To validate the rotor durability against the risk of premature fatigue failure, a 3rd laboratory test facility was set up, Fig. 18. The cyclic rotor centrifugal loading during the life time of the motor were simulated by applying equivalent cyclic forces in the rotor radial direction. Each load cycle is representative of the rotor load variation as the rotor is accelerated from a low/idle speed to its rated maximum working speed, i.e. 15 krpm, and decelerated back to the low/idle speed. The aim of the test was to verify the rotor fatigue life, particularly that of the fir-tree-root connection between the electrical-steel pole segments and the stainless-steel support hub.

The fatigue test results suggest that the rotor pole segments and the support hub will survive more than 8 times the rotor fatigue life design target. Such a rotor durability target was selected and agreed with the vehicle manufacturer, and is a conservative estimation of the rotor "low/idle to maximum working speed" excursions likely to be experienced by the rotor during the life time of the vehicle.

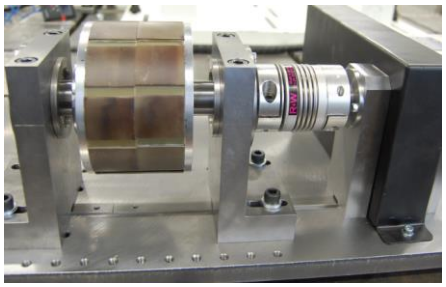

(a)

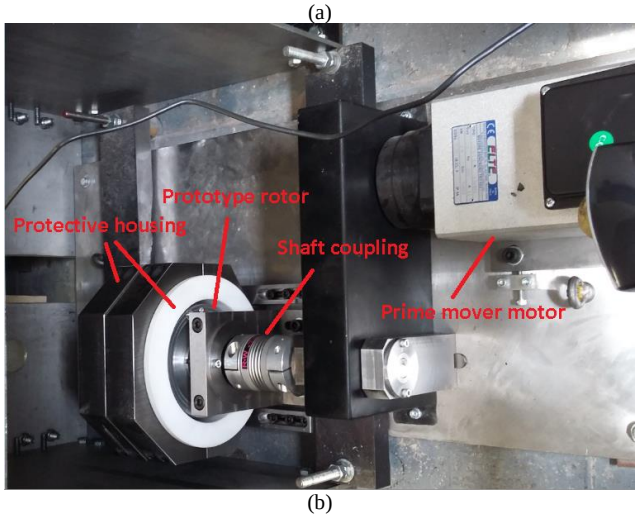

(b)

Fig. 17. Test set up for the rotor over speed evaluation. (a) Rotor comprised of 2 axial sections, and shaft coupling. (b) Complete set up, including the prime mover and protective housing.

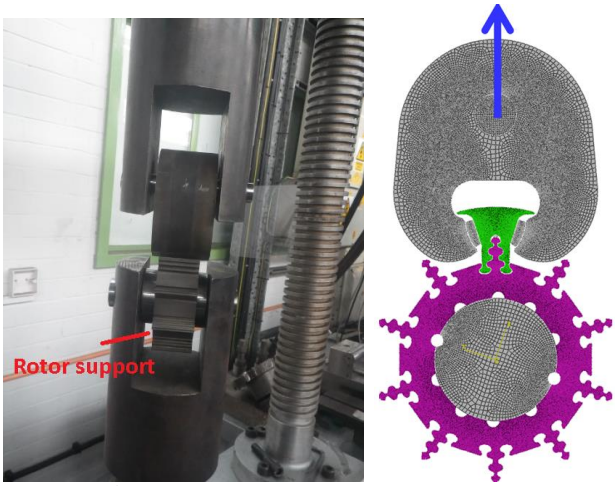

Fig. 18. Rotor fatigue testing under cyclic loading.

V. Conclusions

This paper presented a multi-disciplinary investigation of the rotor support material as part of a low cost high performance ferrite motor. The high-speed rotor structural performance was shown to benefit from the use of non-magnetic metals of higher Young's modulus and yield strength, especially austenitic stainless steels. A work-hardening treatment to the rotor support material also proves to be desirable. It was shown that even a small degree of work hardening can strengthen most grades of stainless steel to fulfill the structural demands of the proposed motor design, without a noticeable change of the magnetic permeability and electromagnetic performance of the motor. Despite the higher thermal conductivity of the copper beryllium compared to austenitic steels, its thermal advantages are minimal when distributed windings are used, and/ or cooling means other than direct rotor shaft cooling are applied. In terms of cost for high volume production, it was shown that the austenitic steel can be 3~6 times cheaper than the state of the art, which may, significantly, boost the cost competitiveness of the low cost ferrite motors. To validate the design performance based on the selected rotor support material, three sets of prototypes were built based on which the BEMF and torque, the rotor integrity up to 120% of the top speed, and the fatigue durability were shown all to meet or exceed the design requirements. This paper is expected to provide a better insight for the designers on how different materials in the rotor support may influence the multi-physical performance and cost of a spoke type electric motor, when designing for a high volume production target.

Acknowledgment

The authors gratefully acknowledge the motivation and support from Jaguar Land Rover under the Evoque-E project.

References

[1] D.Dorrell, L.Parsa, and I.Boldea, "Automotive Electric Motors, Generators, and Actuator Drive Systems With Reduced or No Permanent Magnets and Innovative Design Concepts," IEEE Transactions On Indus Elects, Vol. 61, No. 10, pp 5693 - 5695, Oct 2014.

[2] J. D. Widmer, R. Martin, and M. Kimiabeigi, "Electric vehicle traction motors without rare earth magnets," Sustainable Materials and Technologies (Elsevier), Feb 2015.

[3] T. Raminosoa, A. El-Refaie, D. Pan, K. Huh, J. Alexander, K. Grace, S. Grubic, S. Galioto, P. Reddy,"Reduced Rare-Earth Flux Switching Machines for Traction Applications," Accepted to be published in IEEE Transactions on Industry Applications, 2015.

[4] Li, Y. Li, and B. Sarlioglu, "Partial irreversible demagnetization assessment of flux-switching permanent magnet machine using ferrite permanent magnet material" IEEE Trans. Magn., vol. 51, no. 7, pp. 1–9, July. 2015.

[5] Y. Deshpande and A Toliyat.,"Design of an Outer Rotor Ferrite Assisted Synchronous Reluctance machine (Fa-SynRM) for Electric Two Wheeler Application," IEEE Energy Conversion Congress and Exposition (ECCE), Sep. 2014, pp. 3147 - 3154.

[6] E. Carraro, M. Degano, and N. Bianchi, "Permanent Magnet Volume Minimization in Permanent Magnet Assisted Synchronous Reluctance Motors," in Proc. IEEE Int. Conf. EVER, Monte Carlo, Monaco, Mar. 27-30, 2013, pp 1-4.

[7] S. Morimoto, S. Ooi, Y. Inoue, and M. Sanada, "Experimental Evaluation of a Rare-Earth-Free PMASynRM With Ferrite Magnets for Automotive Applications,'' IEEE Trans. Ind. Electron., vol. 61, no. 10, Oct. 2014.

[8] B. Boazzo, A. Vagati, G. Pellegrino, E. Armando, and P. Guglielmi, "Multipolar Ferrite-Assisted Synchronous Reluctance Machines: A general design approach," IEEE Trans. Ind. Electron., vol. 62, no. 2, pp. 832-845, Feb. 2015.

[9] M. Barcaro and Nicola Bianchi, "Interior PM Machines Using Ferrite to Replace Rare-Earth Surface PM Machines" IEEE Trans. Ind. Appl., vol. 50, no. 2, pp. 979-985, Mar/ Apr. 2014.

[10] A. Vagati, B. Boazzo, P. Guglielmi, and G. Pellegrino, "Design of ferrite assisted synchronous reluctance machines robust toward demagnetization," IEEE Trans. Ind. Appl., vol. 50, no. 3, pp. 1768–1779, May/Jun. 2014.

[11] W. Zhao, T. A. Lipo, and B. I. Kwon, "Comparative Study on Novel Dual Stator Radial Flux and Axial Flux Permanent Magnet Motors With Ferrite Magnets for Traction Application," IEEE Trans. Magn., vol. 50, no. 11, pp. 1–4, Nov. 2014.

[12] M. M. Rahman, K. T. Kim, and J. Hur, "Design and Optimization of Neodymium-Free SPOKE-Type Motor With Segmented Wing-Shaped PM," IEEE Trans. Magn., vol. 50, no. 2, pp. 865–868, Feb. 2014.

[13] W. Fei, W. Liang, and P. C. K. Luk, "Influence of magnet layer number on electromagnetic performance of ferrite interior permanent magnet synchronous machine", International Conference on Electrical Machines and Systems (ICEMS), Oct 2014, pp. 1 – 7.

[14] W. Kakihara, M. Takemoto, and S. Ogasawara, "Rotor structure in 50 kW spoke-type interior permanent magnet synchronous motor with ferrite permanent magnets for automotive applications," in Proc. IEEE Conversion Congress and Exposition (ECCE), Sep. 2013, pp. 606–613.

[15] J. Galioto, P. B. Reddy, A. M. EL-Refaie, "Effect of Magnet Types on Performance of High Speed Spoke Interior Permanent Magnet Machines Designed for Traction Applications," in Proc. Energy Conversion Congress and Exposition (ECCE), Sep 2014, pp. 4513 - 4522.

[16] Y. Burkhardt, A. Spagnolo, P. Lucas, M. Zavesky, P. Brockerhoff, "Design and analysis of a highly integrated 9-phase drivetrain for EV applications," International Conference on Electrical Machines and Systems (ICEMS), Sep 2014, pp. 450 – 456.

[17] M. Kimiabeigi, J. D. Widmer, R. Long, Y. Gao, J. Goss, R. Martin, T. Lisle, J.M. Soler Vizan, A. Michaelides, and B. Mecrow, "High Performance Low Cost Electric Motor for Electric Vehicles Using Ferrite Magnets," Accepted to be published in IEEE Trans. Ind. Electron., June. 2015.

[18] "Permanent Magnet Rotor for High Speed Motors and Generators," by Carl J. Heyne, Granted on May 1986, US4588914 A, Available: http://www.google.com.ar/patents/US4588914.

[19] L. Cunningham, "Beryllium Recycling in the United States in 2000," U.S. Department of the Interior, U.S. Geological Survey (USGS), pp. 6–13, 2004, Available: http://pubs.usgs.gov/circ/c1196p/c1196p.pdf

[20] S. Jewell and S. M. Kimball, "Mineral commodity summaries," U.S. Department of the Interior, U.S. Geological Survey (USGS), 196 p., 2015, Available: http://dx.doi.org/10.3133/70140094

[21] A. Darby and D. Fishwick, "A review of the health effects and the evidence for screening or surveillance in workers exposed to beryllium," Health and Safety Laboratory, Health and Safety Executive (HSE), 2011, Available: http://www.hse.gov.uk/research/rrpdf/rr873.pdf

[22] T.P. Taylor, M. Ding, D.S. Ehler, T.M. Foreman, J.P. Kaszuba, N.N. Sauer, "Beryllium in the environment: a review", Journal of Environmental Science and Health , pp. 439–469, 2003.

[23] K. Mumtaz, S. Takahashi, J. Echigoya, et al, "Magnetic measurements of martensitic transformation in austenitic stainless steel after room temperature rolling," Journal of Materials Science, Vol. 39, 2004, pp. 85– 97.
[24] C. B. Post and W. S. Eberly, "Stability of Austenite in Stainless Steel," Trans. American. Society. Metals., vol. 39, pp. 868- 890, 1947.
[25] Y. Gao, R. Long, Y. Pang, andM. Lindenmo, "Fatigue properties of an electrical steel and design of EV/HEV IPM motor rotors for durability and efficiency," presented at the SAE, Tech. Paper 2010-01-1308.
[26] The Hendrix group, [Online], Available: http://hghouston.com/resources/material-property-data/stainless-steel-data/cold-working-properties.aspx.
[27] Carpenters stainless steel blue book, Selection Alloy Data Fabrication, 2012, page 21, [Online], Available: http://www.cartech.com/techarticles.aspx?id=1476.
[28] A.M. EL-Refaie, "Fractional-Slot Concentrated Windings Synchronous Permanent Magnet Machines: Opportunities and Challenges," IEEE Trans. Ind. Electron., vol. 57, no. 1, pp. 107–121, Jan. 2010.
[29] A. M. EL-Refaie, J. P. Alexander, S. Galioto, et al, "Advanced High Power-Density Interior Permanent Magnet Motor for Traction Applications", Accepted to be published in IEEE Transactions on Industry Applications, 2014.
[30] Shanghai metals market, [online], Available: http://www.metal.com/metals/productinfo/201102250135
[31] MetalPrices.com, [online], Available: http://www.metalprices.com/metal/stainless-steel/stainless-steel-flat-rolled-coil-316
[32] AK Steel, [Online], Available: http://www.aksteel.com/pdf/markets_products/stainless/Stainless_Steel_Price_Book_20140902.pdf